80 FRACTURE ANALYSIS OF CONCRETE PLANE-STRESS PULL-OUT TESTS

V. ČERVENKA and R. PUKL
Klokner Institute of the Czech Technical University, Prague, Czechoslovakia
R. ELIGEHAUSEN
Institute for Building Materials, Stuttgart University, Germany

Abstract
This paper reports on a parameter study which was performed for the Round Robin Analysis Of Anchor Bolts organized by RILEM Committee TC-90 FMA (Fracture Mechanics Applications). 18 plane-stress pull-out specimens were analyzed by the computer program SBETA which is based on the finite element method and takes into account nonlinear fracture mechanics. A simplified formula for the design of such anchors is derived.
Keywords: Pull-Out Test, Anchor Bolt, Non-linear-fracture Mechanics, Finite Element Method.

1 Introduction

The authors have performed a numerical study in connection with the RILEM Round Robin Analysis Of Anchor Bolts [1]. A part of this study, which concerns the plane stress solution, is described in this paper. The plane stress anchor represents a linear anchoring element which can be a steel profile or a row of anchoring bolts. The failure mechanism of anchors subjected to a pull-out load is a complex problem which is typically investigated experimentally. Recent advances in the computational fracture mechanics make it possible to perform a computer simulation of such tests.

2 Description of pull-out tests

A two-dimensional specimen with a steel anchor as shown in Fig.1 is considered. The specimen is supported by two roller bearings and an axial loading force is applied to the anchor. Two cases of lateral constraints were considered, namely, with rigid constraint and without constraint. The thickness of the specimens is 100 mm. The material parameters are specified in Fig.1. The aim of the test was to determine the maximum load which can be transmitted by the anchor under variable geometry and constraint conditions. Three values of the embedment depth d and three ratios of the support span a to the embedment depth are considered. By varying the geometrical parameters and two lateral constraint conditions 18 cases are obtained. All these tests were simulated by computer analysis. This

Fracture Processes in Concrete, Rock and Ceramics Edited by J.G.M. van Mier, J.G. Rots and A. Bakker.
 ISBN 0 419 15870 7

numerical study is in detail described in the report [4].

3 Method of FE-fracture analysis

The analysis was performed by the computer program SBETA which is based on the finite element analysis and a non-linear-elastic constitutive model of concrete. A smeared material approach based on the Bazant's crack-band model [5] is used. The stress-strain law for concrete in tension is bi-linear with a linear part up to the tensile strength and linear softening, Fig.2. In order to model correctly the discrete nature of cracking the softening modulus E_t is related to the fracture energy parameter G_f, the crack band width h and the tensile strength f_t by the formula

$$E_t = -f_t^2 \frac{h}{2G_f} \tag{1}$$

The crack band width is related to the mesh size by $h = \sqrt{A}$, where A is the finite element area. Two types of crack model are used. In the fixed-crack model the crack direction is determined at the instant of crack initiation and kept fixed during the analysis. The shear strain on the crack plane can arise and thus the shear stiffness as defined by Eq.(2) is used. The shear stiffness is modeled by Kolmar's relation [6] in which the shear modulus G declines with the crack band strain ϵ_u:

$$G = r_s \, G_c \, , \qquad r_s = 0.0923 \; ln\left(\frac{\epsilon_u}{5.33}\right) \tag{2}$$

In this formula G_c is the initial shear modulus of concrete and r_s is the reduction coefficient. In the rotated-crack model the crack direction coincides with the principal strain axes. The material properties are modeled only by the normal stress components and the shear stiffness is not used.

The model contains also other properties to describe the concrete behavior, namely, a bi-axial failure function, a non-linear response in compression and a reduction of the compressive strength in cracked concrete. However, these aspects of the SBETA constitutive model are not important for the brittle mode of failure treated here and therefore shall not be discussed in detail. A four-node quadrilateral finite element is used. It is composed of two four-node subtriangles with an exact stiffness integration. The nonlinear solution is performed by the arch-length method which enables the analysis of the post-peak behavior. Details about the program SBETA can be found in references [2,3]).

4 Results of parameter study

The subject of the parameter study was to simulate 18 cases of pull-out tests described in Section 2. An example of a finite element mesh for the pull-out specimen is shown in Fig.3. Note that only half of the specimen was analyzed taking advantage of the symmetry. Similar meshes were used for all specimens. All cases were calculated for fixed and rotated crack models. The calculated peak loads are given in Table 1. It contains also the data from an analysis based on the

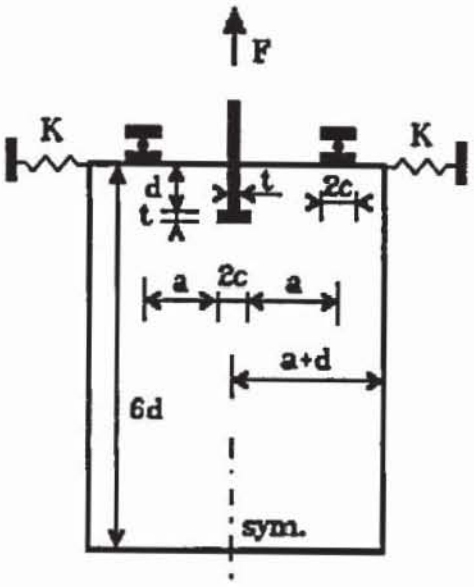

Geometry:
$d = 50, 150, 450$ mm
$a = d/2,\ d,\ 2d$
$2c = 3d/10,\ t = d/10$
thickness = 100 mm

Lateral constraint: $K = 0, \infty$

Material properties:
$f_t = 3$ MPa, $f_c = 40$ MPa,
$E = 30$ GPa, $\nu = 0.2$
$G_f = 100$ N/m

Fig.1 Geometry and material properties of the pull-out specimens.

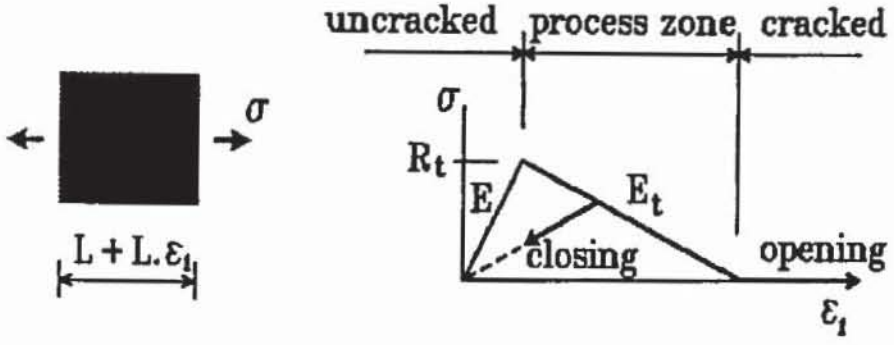

Fig.2 Stress-strain law for concrete in tension.

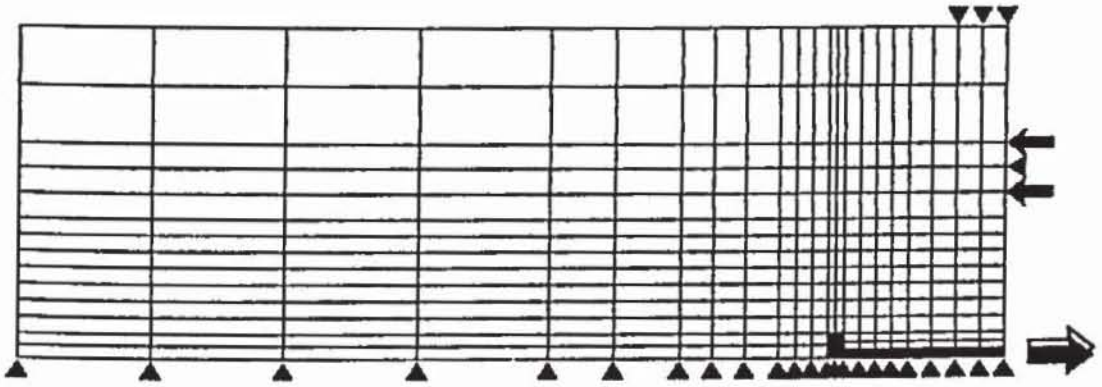

Fig.3 Finite element mesh for typical specimen.

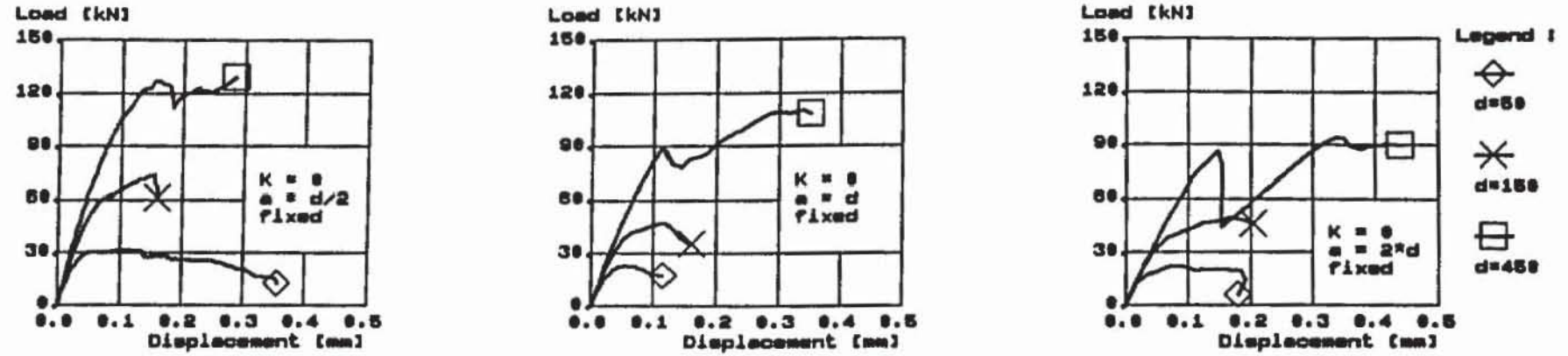

Without lateral constraint.

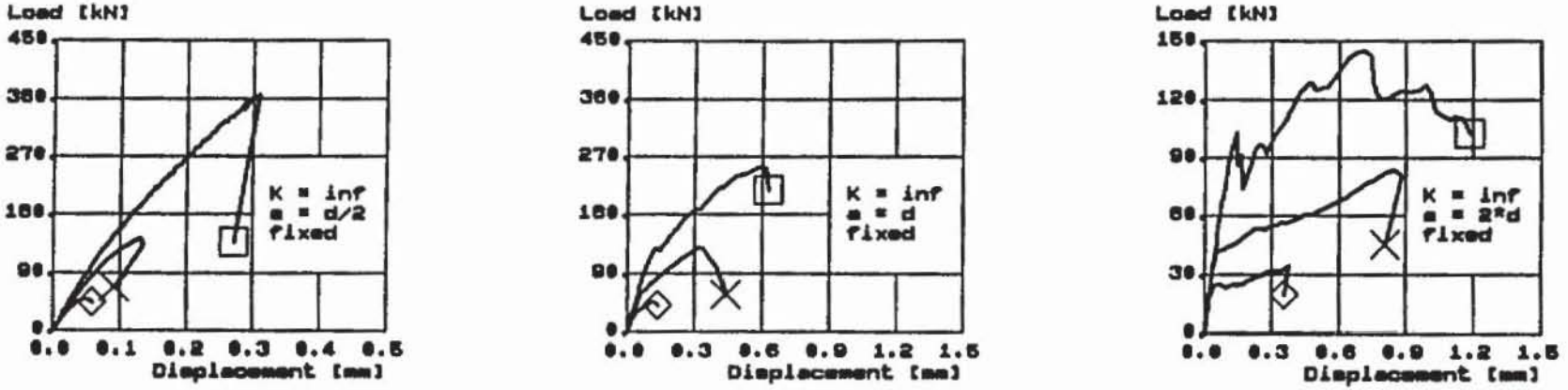

With lateral constraint.

Fig.4 Load-displacement diagrams of 18 specimens analyzed by fixed crack model.

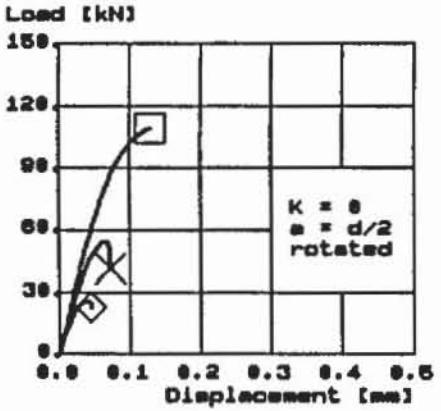

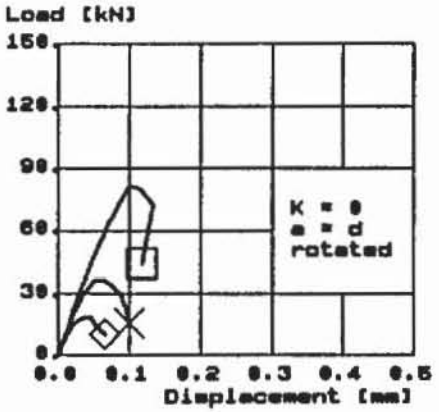

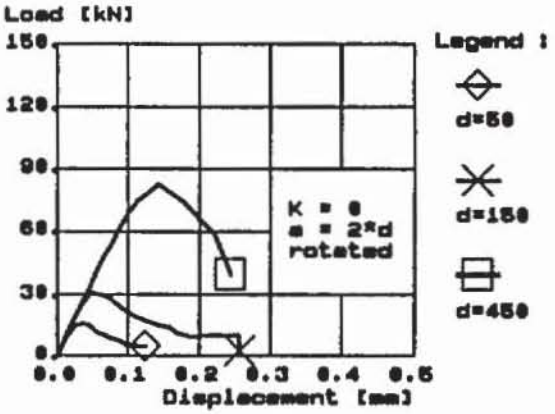

Without lateral constraint.

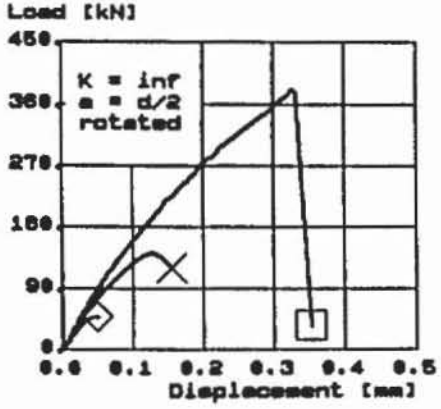

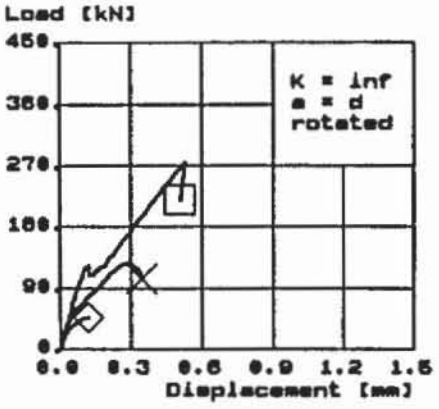

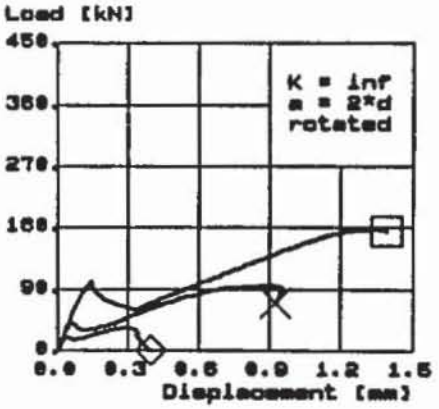

With lateral constraint.

Fig.5 Load-displacement diagrams of 18 specimens analyzed by rotated crack model.

microplane model which will be discussed later. Table 2 summarizes displacements of the anchor head at peak load. The load-displacement diagrams for fixed-crack analysis of all specimens are shown in Fig.4 and for rotated-crack analysis are shown in Fig.5. (Note that different scales of the diagrams are used. This had to be accepted because of the wide range of the loads, varying from 16.6 to 382.7 kN.)

Table 1 Peak loads [kN]

lateral constraint		0			∞		
d [mm] =		50	150	450	50	150	450
a =	material model						
d/2	fixed cracks	31.9	74.3	129.4	49.8	144.6	366.5
	rotated cracks	26.0	54.3	109.0	49.5	142.7	382.7
d	fixed cracks	23.1	47.2	110.2	47.6	130.7	254.9
	rotated cracks	18.8	36.5	81.9	47.1	129.3	276.1
	microplane	17.5	42.7	93.4	-	-	-
2 d	fixed cracks	22.2	49.5	94.3	34.6	84.0	145.5
	rotated cracks	16.5	31.1	82.9	34.3	96.8	179.6

Table 2 Displacements [mm] of anchor head at peak load

lateral constraint		0			∞		
d [mm] =		50	150	450	50	150	450
a =	material model						
d/2	fixed cracks	0.102	0.154	0.284	0.047	0.130	0.308
	rotated cracks	0.035	0.067	0.123	0.045	0.125	0.325
d	fixed cracks	0.053	0.107	0.338	0.111	0.316	0.585
	rotated cracks	0.035	0.050	0.100	0.104	0.287	0.527
	microplane	0.034	0.087	0.186	-	-	-
2 d	fixed cracks	0.071	0.164	0.336	0.378	0.843	0.704
	rotated cracks	0.034	0.046	0.141	0.280	0.911	1.322

The most diagrams have only one peak at the maximum load. However, some specimens reached first local instability before maximum load, then, after forming a new stable crack pattern the load could be further increased up to the peak. The post-peak descending branch could be calculated until a kinematically unstable system was reached (pulling-out of the anchor).

Each diagram containing three curves shows the effect of the embedment depth (size effect) on the pull-out behavior of the specimens. It can be observed that the ratio of the failure loads for the specimens with the geometrical scaling factor 3 is much smaller than this value. This effect will be quantitatively evaluated in Section 5. From comparison of the different diagrams the effect of the various

parameters can be observed. The tests with lateral constraint gave always greater maximum loads than tests without constraint. With increasing support span the maximum load decreases and the effect of lateral constraint also decreases.

The effect of the crack model can be found from the comparison of Fig.4 and 5. A comparison for a particular case (d=450 mm, a=d, k=0) is shown in Fig.6. Here the fixed crack model gives a higher maximum load than the rotated crack model. This could be expected because the rotated-crack model is by it's nature more flexible. It is also interesting to compare these models with an analysis based on the microplane model which was performed by Ozbolt for the same Round-Robin Analysis [1]. The microplane model considers a discrete material structure [7]. It appears that the microplane model gives an intermediate solution between fixed and rotated crack models.

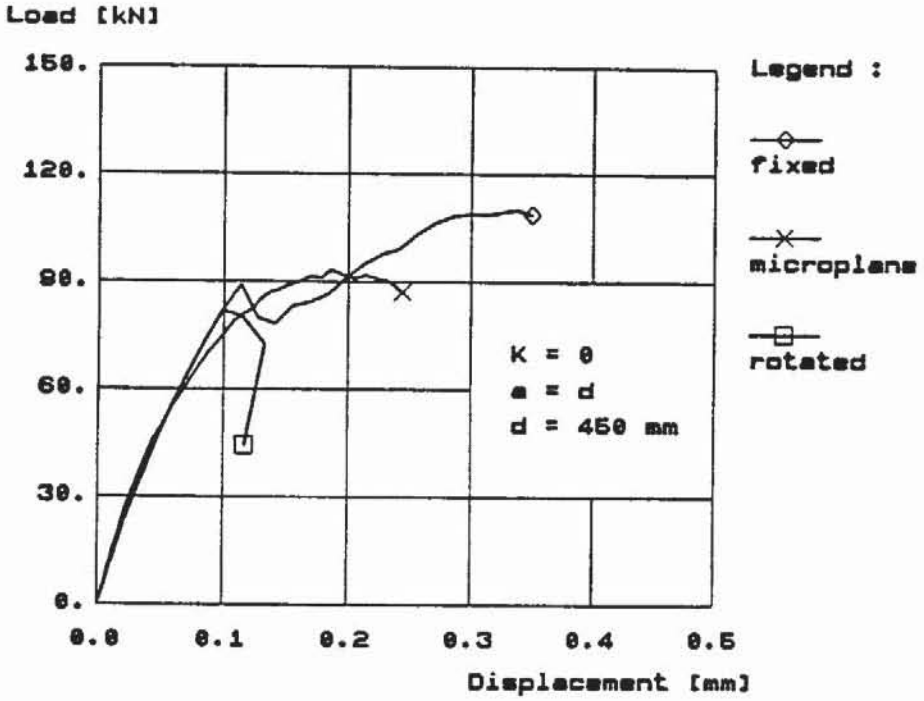

Fig.6 Comparison of load-displacement diagrams for three crack models.

However, the fixed-crack model is not always stronger (see Table 1). E.g. in constrained specimens with d=450 mm the rotated crack analysis gave greater maximum loads than the fixed crack one. Thus a general conclusion about the relation between fixed and rotated crack analysis with respect to the maximum load cannot be made.

The computer simulation provided also a large amount of information about the deformed states, crack patterns and stress fields. They were evaluated using the SBETA graphical system and are comprehensively described in the report [4]. Here one example of the crack propagation is shown only. Fig.7 illustrates the crack development for a typical specimen. In the bottom the crack process zone is depicted by crack-lines, while in the upper part of the figure the crack is indicated by means of strain isolines. Both of these graphical forms are useful for the

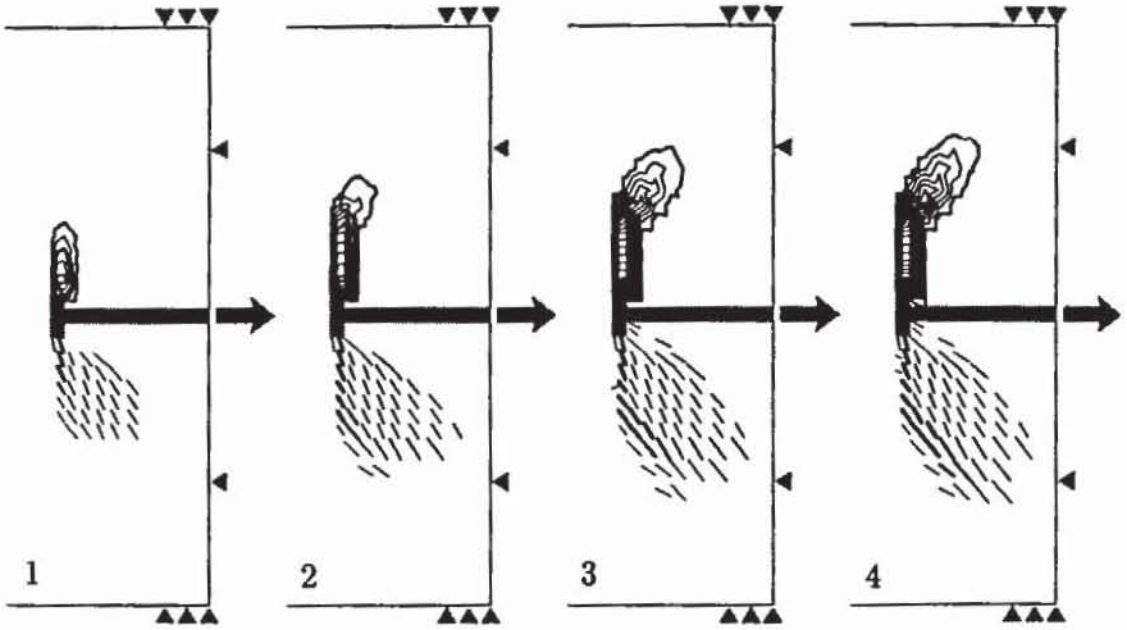

Fig.7 Crack propagation calculated by SBETA for the specimen d=50 mm, a=d, fixed crack model.

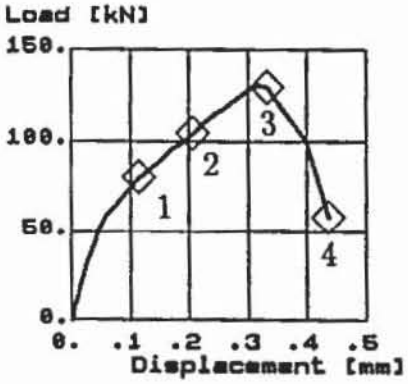

Fig.8 Load-displacement diagram for the specimen from Fig.7.

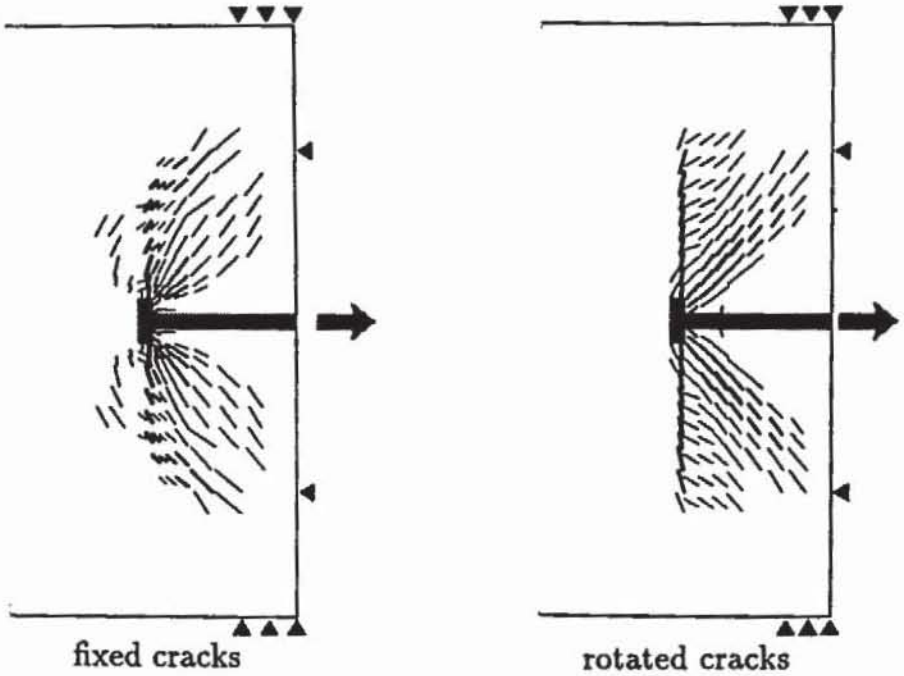

Fig. 9 Comparison of the final crack patterns for two crack models ($K = \infty$).

investigation of the crack localization. Fig.8 shows the corresponding load-displacement diagram with locations of points for crack patterns (total number of load steps was 26). In Fig.9 the final crack patterns for fixed and rotated crack analyses are compared.

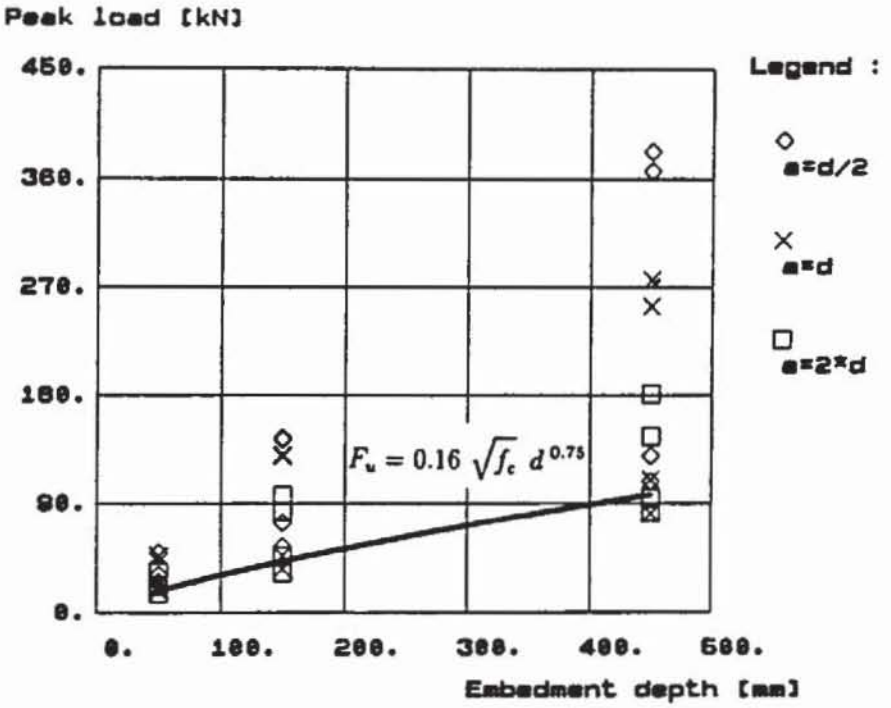

Fig.10 Comparison of Eq.(4) with all simulated tests.

5 Size effect

Some practical conclusions can be drawn from this parameter study for the design of linear anchors in plane stress state. A formula for the maximum load can be proposed in the following form:

$$F_u = k\sqrt{f_c}\, d^{\alpha} \left(\frac{a}{d}\right)^{\beta} \tag{3}$$

Failure load F_u is in kN. The embedment length d and the support span a are in mm. The thickness is considered as $b = 100$ mm. In the calculation $f_c = 40$ MPa. In Eq.(3) the effect of concrete strength on F_u is represented by the expression $\sqrt{f_c}$. This is based on the generally accepted assumption that the the pull-out failure load is directly related to the tensile strength of concrete which is approximately proportional to this expression $\sqrt{f_c}$. However, recent investigation on the behavior of anchors indicate that the concrete cone failure load is proportional to the parameter $\sqrt{EG_f}$ [8]. A more general expression could be derived by a similar numerical study with variation of the parameters E and G_f.

Constants k, α, β were derived using the least-square fit method. For specimens without lateral constraint they amount to: $k = 0.25, \alpha = 0.68, \beta = -0.28$ and for specimens with lateral constraint: $k = 0.31, \alpha = 0.80, \beta = -0.40$. The results

indicate that for a large span the effect of lateral constraint vanishes. Using Eq.(3) and the above given parameters this occurs at $a/d \doteq 5$. In such a case the expression $k(a/d)^{\beta}$ is equal to 0.16. This corresponds to practical cases with large support spans. Thus Eq.(3) can be simplified as

$$F_u = 0.16 \sqrt{f_c}\ d^{0.75} \tag{4}$$

The formula is compared with the simulated tests in Fig.10. The exponent $\beta = 0.75$ in Eq.(4) is half way between the values valid for linear fracture mechanics ($\beta = 0.5$) and theory of plasticity ($\beta = 1.0$). Before practical implementation of the above results an experimental verification should be made at least for some representative cases.

6 Conclusion

The computer simulation of pull-out tests based on the finite element method and nonlinear fracture mechanics was successfully applied. A simple formula for the maximum pull-out force of the linear anchors in plane stress state is derived.

References

[1] ELFGREN, L. (Editor) - Round-Robin Analysis of Anchor Bolts, RILEM TC-90 FMA Fracture Mechanics of Concrete-Application, Preliminary Report, Luleå University of Technology, September 1990.

[2] ČERVENKA, V., ELIGEHAUSEN, R., PUKL, R. - SBETA Computer Program For Nonlinear Finite Element Analysis of Concrete Structures, Part 1, Program Description, Part 2, User's Manual, Part 3, Examples of Applications, Mitteilungen des Instituts für Werkstoffe im Bauwesen No.1990/1, Universität Stuttgart.

[3] ČERVENKA, V., ELIGEHAUSEN, R., PUKL, R. - FEM Computer Models Of Concrete Structures, IABSE Colloquium Structural Concrete, April 10-12, 1991, Stuttgart, Germany.

[4] PUKL, R., ČERVENKA, V., ELIGEHAUSEN, R. - Study of pull-out tests of anchor bolts - 2D computer simulation, Institut für Werkstoffe im Bauwesen, Universität Stuttgart, 1991 (Report under preparation)

[5] BAŽANT, Z.P., OH, B.H. - Crack Band Theory for Fracture of Concrete, Mater. Struct. RILEM, Paris, France, 16, 1983, pp. 155-177.

[6] KOLMAR, W. - Beschreibung der Kraftübertragung über Risse in nichtlinearen Finite-Element-Berechnungen von Stahlbetontragwerken, Dissertation, Technische Hochschule Darmstadt 1985, p.94.

[7] BAŽANT, Z.P., OŽBOLT, J. - Nonlocal microplane model for fracture, damage, and size effect in structures, ASCE Journal of the Engineering Mechanics Division, 116, No.11, Nov. 1990, pp.2485-2505.

[8] OŽBOLT, J., ELIGEHAUSEN, R. - Numerical Analysis of Headed Studs Embedded in Large Plain Concrete Blocks. Institut für Werkstoffe im Bauwesen, Universität Stuttgart, Report No. 4/10-90/9, Oct. 1990.